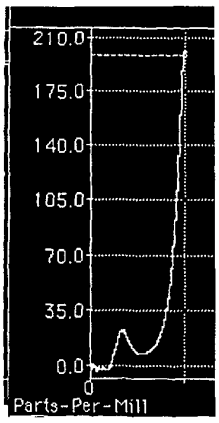

Fig. 9. Experimental result showing premature breakthrough and transient rebound of CO_2 in a cold test canister in cold water. X-axis is time (s) and Y-axis is CO_2 concentration in ppm.

When simulating these conditions with our model, we found that CO_2 in the effluent rose rapidly once CO_2 started flowing and then began dropping as the canister began to warm due to exothermic CO_2 absorption reactions (Fig. 10). However, just as in the experimental case, absorption was not sustained, and CO_2 began once again to climb steadily. Corresponding thermal images are shown in Fig. 11.

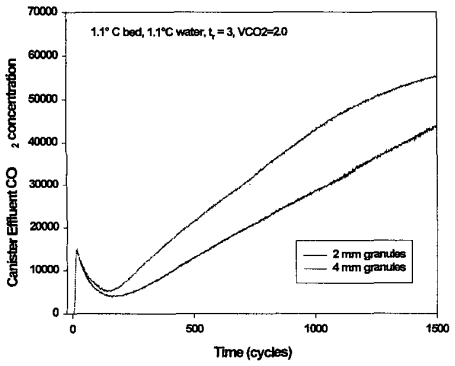

Fig. 10. Simulation result with 33° F canisters containing large and small granules in 33° F water.

Unlike the first image in Fig. 7, the first image in Fig. 11 shows a thoroughly chilled canister. Eventually, CO_2 absorption reactions start to warm the upstream end of the canister, but compared to Fig. 7, these initial reactions, seen in the second image of the sequence, are weak and diffuse. In the third image we see the reaction region has finally consolidated and is actually more intense than in Fig. 7. At this point, CO_2 is being well scrubbed. However, in the fourth image it is apparent that the reaction intensity is not being sustained, and in the last image the reactions are dissipated and are of relatively low intensity.

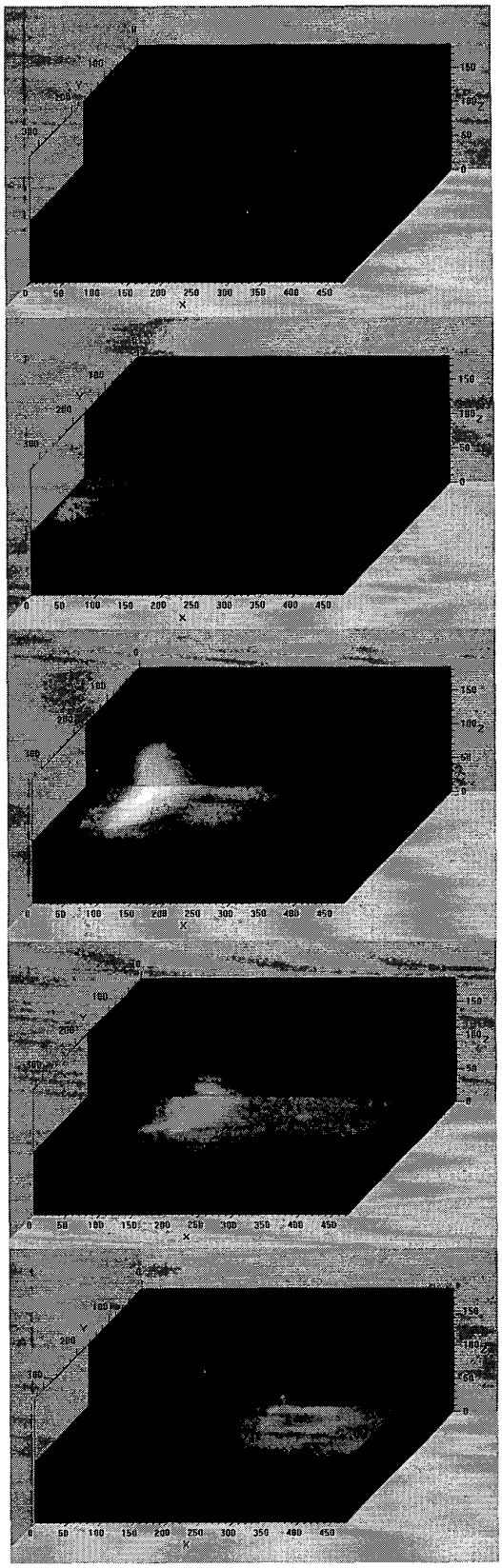

Fig. 11. Thermal images in a chilled canister.

In the following sequence, thermal conductivity and heat transfer coefficient within the canister were reduced by a factor of 10 from 1 W/m · °C to 0.1 W/m · °C.

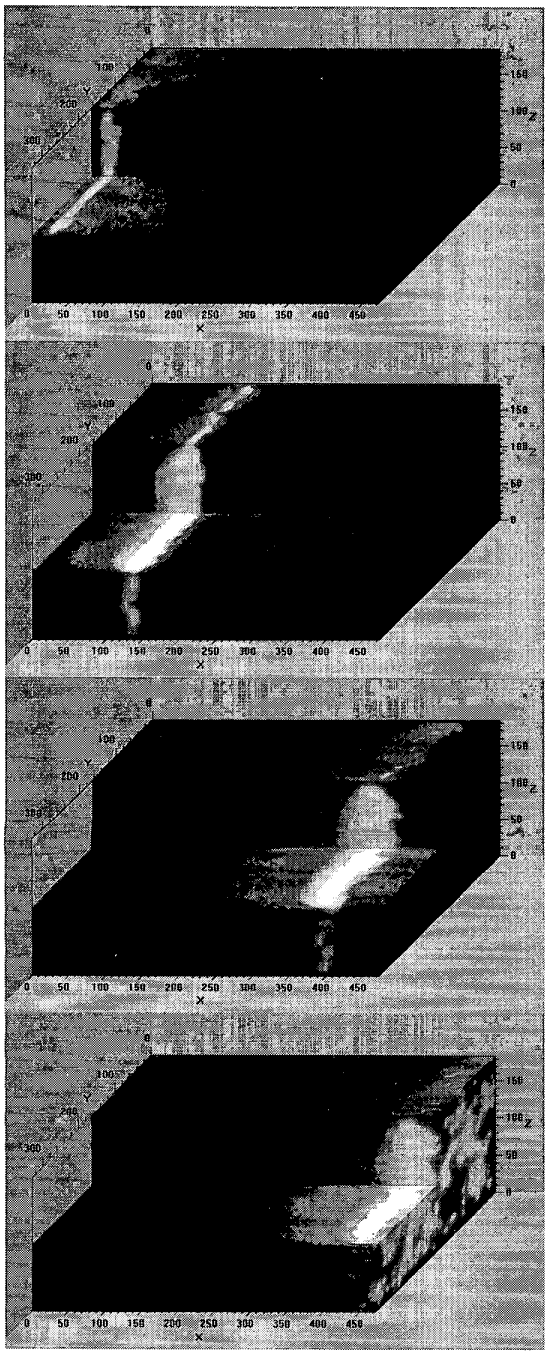

Fig. 12. When thermal conductivity and the heat transfer coefficient are reduced to 1/10 their previous value, the intense reaction front, once established, is sustained.

Fourier's law of conduction,

$$\dot{Q} = -k \cdot A \cdot \frac{dT}{dx}$$

where $\dot{Q}$ is heat flux, A is the cross-sectional area normal to the heat flux, and $\frac{dT}{dx}$ is the temperature gradient, explains why the reaction intensity shown in Fig. 11 was not sustained, whereas in Fig. 12 it was.

In the original condition of the cold canister with a thermal conductivity of 1 W/m · °C the combination of large thermal gradients and high thermal conductivity causes a high rate of heat transfer which removes heat from the reaction front faster than it can be generated by exothermic reactions. The net result is reaction front cooling and diminished reactivity. Convective heat loss also contributes to cooling and diminished reactivity.

Although it is not feasible actually to reduce thermal conductivity and the heat transfer coefficient in a scrubber canister by a factor of 10, simulating that intervention using the computer model is straightforward.

B. Cylindrical Canisters

Cylindrical canisters can be modeled with only a slight reduction in computational efficiency. In Fig. 13 we see a short cylindrical canister approaching depletion in cold water.

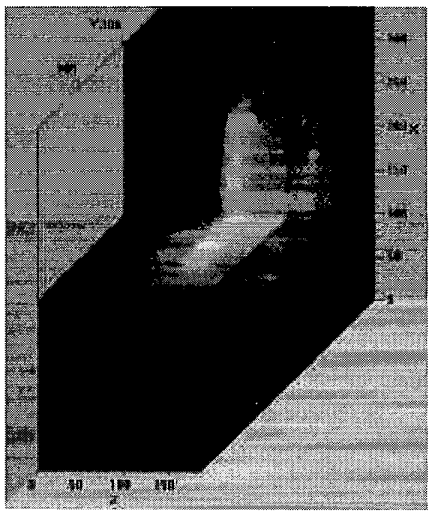

Fig. 13. Short cylindrical axial flow canister.

Fig. 14 shows the largest cylindrical canister modeled to date. It contains 250,000 cells and requires a full megabyte of computer memory to run. With a 1.4 GHz Intel processor each simulation run takes approximately 12 hours.

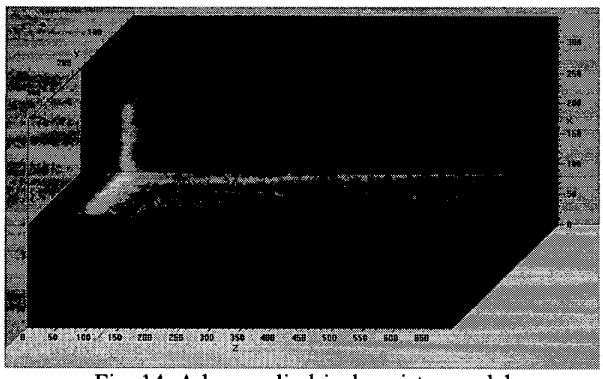

Fig. 14. A long cylindrical canister model.

C. Thermal Curves

The simulation allows us to monitor temperatures anywhere within the canister, as well as average granule and gas temperatures. In Fig. 15 we see four simulated

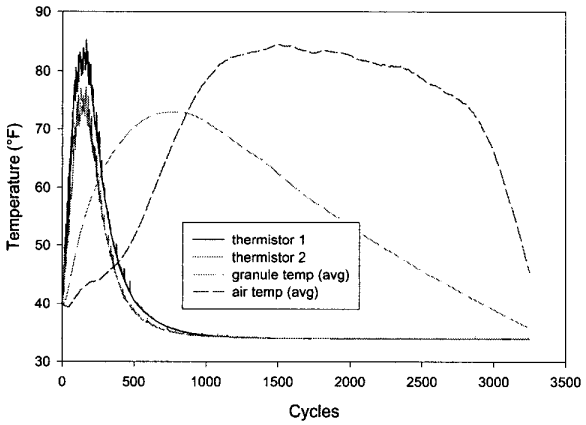

Fig. 15. Time course of various canister and gas temperatures.

thermistor recordings. On the far left are two "thermistors" located close to the flow inlet of the canister, one located centrally, and one peripherally. CO_2 absorption reactions start upstream, and thus temperature rises early and then falls as the reaction front moves downstream. In this example, average granule temperature peaked at a time corresponding to about 700 computing cycles (Cycles) then dropped almost linearly. The average gas temperature plateaued before plummeting as the canister became completely depleted.

V. CONCLUSIONS

The model replicates the essential features of CO_2 scrubber kinetics, including the effects of temperature, residence time, and canister packing. It replicates the complex non-sustaining reaction front behavior in cold canisters and provides a means for experimentally altering model parameters to search for mechanisms of canister behavior.

The ability to study temperature curves is currently helping NEDU devise strategies for estimating remaining scrubbing time based on canister temperature.

Analysis of the statistical properties of thermal fluctuations, akin to studies of nonequilibrium statistical mechanics, may give us an indirect measure of transport coefficients. Those coefficients may in turn improve our predictions of canister failure, or help us rapidly assess the benefit of changes in canister design or absorbent properties. That analysis will be much easier to conduct in the simulation than in actual canisters.

We anticipate that as yet unforeseen uses for a simulation of canister dynamics should manifest themselves in the near future.

REFERENCES

[1] *U. S. Navy Unmanned Test Methods and Performance Goals for Underwater Breathing Apparatus,* Navy Experimental Diving Unit Technical Manual 01-94, 1994.

[2] J.R. Clarke, "Statistically based CO2 canister duration limits for closed-circuit underwater breathing apparatus", U.S. Navy Experimental Diving Unit, Report 2-99, 1999.

[3] Occupational Safety and Health Administration. "Dixie Divers, Inc; Grant of Permanent Variance", *Federal Register*, vol. 64, pp. 712432-71261, Dec. 20, 1999.

[4] L.C. Graton and H.J. Fraser, "Systematic packing of spheres with particular relation to porosity and permeability", *J Geol.*, vol. 43, pp. 785-909, 1935.